



Cite this: *RSC Adv.*, 2021, 11, 33723

# Development of a pH-sensitive functionalized metal organic framework: *in vitro* study for simultaneous delivery of doxorubicin and cyclophosphamide in breast cancer†

Ragini Singh,<sup>a</sup> Binayak Kumar,<sup>‡a</sup> Ram Krishna Sahu,<sup>‡a</sup> Soni Kumari,<sup>‡a</sup>  
Chandan Bhogendra Jha,<sup>‡b</sup> Nahar Singh,<sup>c</sup> Rashi Mathur<sup>b</sup> and Suresh T. Hedau <sup>\*a</sup>

Exploration of an efficient dual-drug based nanocarrier with high drug loading capacity, specific targeting properties, and long-term stability is highly desirable in cancer therapy. Metal–organic frameworks (MOFs) have proven to be a promising class of drug carriers due to their high porosity, crystalline properties with defined structure information, and their potential for further functionalization. To enhance the drug efficacy as well as to overcome the burst effect of drugs, here we synthesized a pH responsive folic acid (FA) and graphene oxide (GO) decorated zeolitical imidazolate frameworks-8 (GO-FA/ZIF-8), for targeted delivery of doxorubicin (DOX) and cyclophosphamide (CP), simultaneously. In this system, DOX molecules were encapsulated in the pores of ZIF-8 during *in situ* synthesis of ZIF-8 and CP molecules have been captured by the GO surface *via* hydrogen bonding and  $\pi$ – $\pi$  interactions as well. Furthermore, the resulting pH-responsive nanocarrier (DOX@ZIF-8/GO-FA/CP) showed *in vitro* sustained release characteristics (76% of DOX and 80% of CP) by cleavage of chemical bonding and disruption of the MOFs structure under acidic condition (at pH 5.6). Moreover, DOX@ZIF-8/GO-FA/CP has synergistic cytotoxic effects as compared to the combination of both the drugs without ZIF-8/GO-FA when treating MCF-7 and MDA-MB-231 breast cancer cell lines (with a combination index of 0.29 and 0.75 for MCF-7 and MDA-MB-231 cell-lines, respectively). Hence this system can be applied as an effective platform for smart dual drug delivery in breast cancer treatment through its remarkable manageable multidrug release.

Received 14th June 2021  
Accepted 9th October 2021

DOI: 10.1039/d1ra04591a

rsc.li/rsc-advances

## 1. Introduction

Cancer is a serious global health issue that continues to be the world's second leading cause of death. This is said to be the cause of one out of every four deaths.<sup>1</sup> The mortality rate owing to carcinogenic infection is expected to reach 13.1 million by 2030.<sup>2,3</sup> Chemotherapy is the most cost-effective and convenient method for treating cancer among the numerous therapeutic options. However, direct injection of chemotherapeutic drugs has a low therapeutic efficiency and causes undesirable side effects on normal cells.<sup>4</sup> So that, much effort has been made to

design carriers for enhancing the delivery efficiency and reducing the side effects of toxic drugs.<sup>5</sup> The advent of nanotechnology ushered in a new era in drug delivery systems (DDSs), having great potential to overcome the challenges of conventional chemotherapy, such as loading issues, poor bio-distribution, and dose-related side effects. Owing to their high biocompatibility and biodegradability organic based nanocarriers are often used but their low stability and controlled drug release is a challenge.<sup>6–8</sup> Whereas, inorganic nanocarriers, such as gold and mesoporous silica, have a high chemical/physiological stability and multifunctionality, but their biocompatibility and biodegradability are under debate.<sup>9–12</sup>

As compared to the other DDSs, metal–organic frameworks (MOFs) are fascinating materials having many advantages such as, tunable structures, compositions and chemical properties enriched methods of modification and functionality.<sup>13–19</sup> Interestingly, the beneficial physicochemical features of MOFs are unaffected by modification. Beside this, large surface areas and high porosity endow MOFs with high loading capacity of different type of molecules like gas and drugs. Along with this, the weak coordination interaction ensures the biodegradability

<sup>a</sup>Division of Molecular Oncology, ICMR-National Institute of Cancer Prevention and Research, I-7, Sector 39, Gautam Buddha Nagar, Noida-201301, U.P., India. E-mail: suresh.hedau@gov.in; Tel: +91-0120-2446909

<sup>b</sup>Division of Cyclotron and Radiopharmaceutical Sciences, Institute of Nuclear Medicine and Allied Sciences, Defense Research and Development Organization, Brig. S.K. Mazumdar Marg, Delhi 110054, India

<sup>c</sup>CSIR-National Physical Laboratory, New Delhi 110012, India

† Electronic supplementary information (ESI) available. See DOI: 10.1039/d1ra04591a

‡ Equal authorship.



of MOFs. So that, in drug delivery applications, MOF nanoparticles (NPs) with suitable size and surface properties are highly desirable because these factors have significant impact on porosity, colloid stability, drug release profiles and cellular uptake.<sup>20–22</sup> In case of MOFs, metal ions and organic linkers are building blocks. The first thing to consider when choosing MOFs as drug carriers is toxicity. So that, it is necessary that the metal ions and organic ligands used to construct drug-carrying MOFs with good biocompatibility. Some metals, such as Cr and Ni, are highly toxic, and certain metals are essential elements for human life activities, with relatively high content in the human body, such as plasma containing about 22 mM iron and tissues containing zinc (180 mM), copper (68 mM), and manganese (180 mM).<sup>23</sup> Hence, these non-toxic metal ions should be preferred when MOFs are synthesized for drug carriers. Among of them,  $\text{Zn}^{2+}$  is an endogenous metal ion commonly and extensively used to construct MOFs. Zeolitic imidazolate framework-8 (ZIF-8) is a type of nontoxic biocompatible MOF, consisting of inorganic zinc ions acting as nodes connected by 2-methylimidazolate linkers.<sup>24</sup> It combines highly desirable zeolitic and MOF properties such as crystallinity, microporosity, high surface area, and exceptional thermal and chemical stability.<sup>25</sup> Because of the unique property, ZIF-8 is used to construct controlled-release delivery systems for biomolecules (DNA, enzyme, protein, fluorescein),<sup>26–28</sup> as well as for drug molecules.<sup>29–34</sup> It is worth noting that ZIF-8 remains stable under neutral conditions and rapidly degrades in an acid environment due to protonation.<sup>35,36</sup> The superiority of ZIF-8 in biomedical science has also been highlighted in earlier studies.<sup>37,38</sup>

However, the toxicity is the major concern when ZIF-8 is applied in DDSs. Some research stated that undecorated ZIF has high toxicity and product of rapid disintegration is so toxic that it kills animals, which greatly limits its practical applications.<sup>39</sup> As a result, it is highly desirable to regulate MOF biodegradability in order to precisely control MOF disassembly and drug release profile, allowing for proper degradation and removal of nanocarriers when drug delivery is complete. Basically, surface modification is ingenious to fine tune the degradation of materials and improve biocompatibility. To investigate the toxicity of modified ZIF-8 histopathological examinations has been done in some reported studies to analyze major organs including heart, liver, spleen, lung and kidney and they claimed no obvious histologic abnormality has been obtained after treatment with modified ZIF-8.<sup>40–42</sup> Therefore, the urgent thing that we need to do is to modify the surface of MOFs for improving biodegradability when it is used in biomedical applications.<sup>43–45</sup> Although, studies have demonstrated a “ship-in-a-bottle” strategy to encapsulate drug molecules during the synthesis of MOFs with high loading capacity, such as caffeine and DOX which has shown promise in pH-responsive drug delivery.<sup>46,47</sup>

In the lane of DDSs, various limitations such as poor absorption, acquired drug resistance, high drug dosing-related side effects, and rapid renal clearance limit the use of single-drug chemotherapy.<sup>48,49</sup> To overcome these limitations, combination chemotherapy (*i.e.* two or more chemotherapy drugs at

the same time has been used) strategy is gaining wide attention in tumor therapy because of its low side effect and synergistic effect to kill the cancer cell.<sup>50,51</sup> In continuation of combinatorial therapy, different nanoformulations as dual drug delivery systems (DDDSs) have been reported for various drug combinations such as cisplatin and DOX; resveratrol and docetaxel; 10-hydroxycamptothecine and methotrexate; 5-fluorouracil and curcumin; paclitaxel (PTX) and cis-platinum *etc.*<sup>52–56</sup>

In the present work we synthesized graphene oxide (GO) and folic acid (FA) decorated ZIF-8 nanocarrier (DOX@ZIF-8/GO-FA/CP) for delivery of anthracycline (AC) based drug combination of DOX and cyclophosphamide (CP). AC is a common chemotherapy regimen usually given to cure localized breast cancer. In the proposed work an *in vitro* study has been done for simultaneous delivery of DOX and CP with ZIF-8/GO-FA in MCF-7 and MDA-MB-231 cell lines. MCF-7 is a breast cancer cell line having characteristics of estrogen receptor and progesterone receptor gene expression and lack of Her-2 gene expression called hormone receptor positive breast cancer. It covers more than 70% of breast cancer subtype. Whereas MDA-MB-231 is also a breast cancer cell lines are having characteristics of lack of all three genes expression and such category known as triple negative breast cancer which is highly aggressive form and it covers 25% of breast cancer subtype. So that, cell viability has been evaluated in MCF-7 and MDA-MB-231 cancer cell-lines. DOX and CP both damage cancer cells' DNA, preventing them from dividing and ultimately killing them.<sup>57</sup> DOX is widely used to cure breast cancer, however, its dose-related side effects, such as bone-marrow toxicity, gastrointestinal disorders, acute or cumulative cardiotoxicity, and extravasation are the major limitations. In order to minimize the side effects and to enhance the therapeutic efficacy of DOX, functional materials based controlled drug release techniques are highly desirable.<sup>58</sup> To keep in mind the drawback of burst effect in DDSs, we used GO layered sheets with ZIF-8 for delivery of drugs in controlled manner. Furthermore, because cancerous cells are overexpressed with folate receptor, we employed FA functionalized GO to adorn the ZIF-8 for targeted delivery, so that drugs loaded nanocarrier (DOX@ZIF-8/GO-FA/CP) target cancerous cells preferentially. DOX is encapsulated in the pores of ZIF-8 and CP molecules attached to the surface of GO-FA *via* hydrogen bonding and  $\pi$ - $\pi$  interactions. To the best of our knowledge, ZIF-8/GO-FA nanocomposite as a nanocarrier for simultaneous delivery of DOX and CP, has not been reported. We anticipate that this DDS will not only have improved cellular uptake at tumor site, but will also have synergetic cytotoxic effects.

## 2. Experimental

### 2.1 Reagents

2-Methylimidazole (99%),  $\text{Zn}(\text{NO}_3)_2 \cdot 6\text{H}_2\text{O}$  (99%), methanol (HPLC grade), DOX and CP, diethylenetriamine (DETA), *n*-(3-(dimethylamino)propyl)-*n*-ethylcarbodiimide (EDC), *n*-hydroxysuccinimide (NHS), folic acid (FA), graphene oxide (GO), 2',7'-dichlorofluorescein diacetate (DCFDA), propidium iodide (PI) and 3-(4,5-dimethylthiazol-2-yl)-2,5-diphenyltetrazolium bromide (MTT) were purchased from Sigma-Aldrich. DMEM,



FBS and Pen/Strep are procured from Gibco Life Technology and Plastic ware T25-Flask, 6 well plate and 24 well plate purchased from Thermo scientific. MCF-7 and MDA-MB-231 cell line purchased from NCCS-Pune, India.

## 2.2 Instruments

The Fourier transform infrared spectrum (FTIR) was measured by FT-IR, 184 Agilent, model Cary 630. UV-vis spectra were measured with a UV-visible spectrophotometer (PerkinElmer UV-vis spectrometer). X-Ray Diffraction (XRD) patterns were obtained using ECO D8 model advance equipment (Bruker, Germany) using Cu K $\alpha$  (1.5418 Å) radiation. The Fourier transform (FT)-Raman scattering measurements were carried out on a Renishaw inVia-plus micro-Raman system, at room temperature, with 532 nm excitation wavelength. The morphology and elemental composition were studied using LEO 440 scanning electron microscope (SEM) equipped with energy dispersive X-ray spectroscopy (EDS) and transmission electron 178 microscope (TEM, FEI, model F-30 G2 STWIN, Netherland). The charge was determined by using Malvern Zeta sizer, Z90 system.

## 2.3 Synthesis of DDDSs

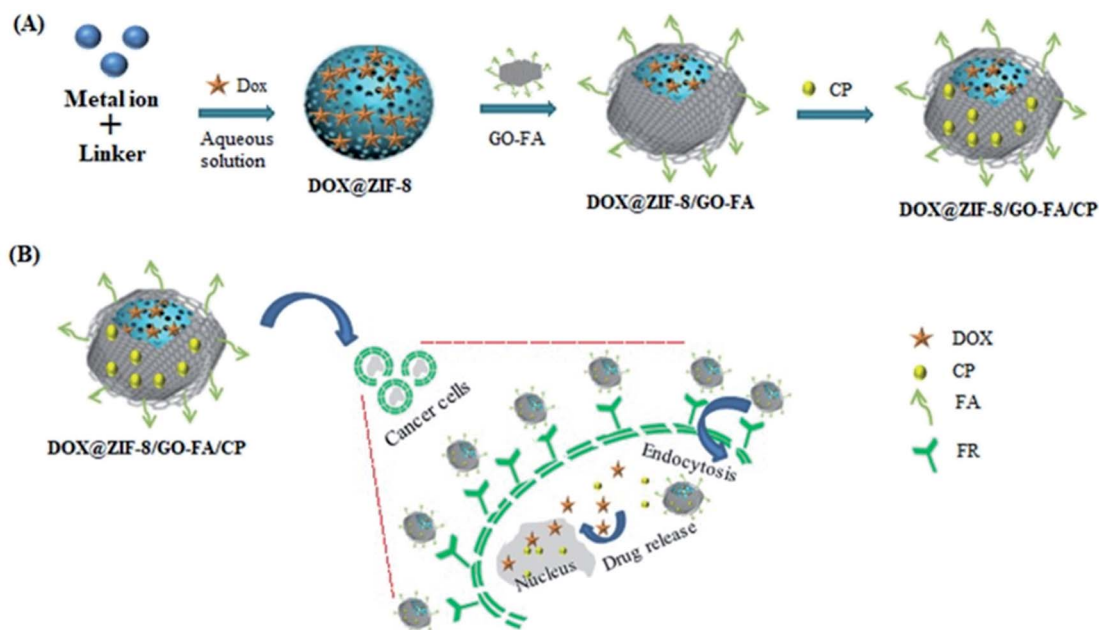
**2.3.1 Functionalization of GO surface with DETA and conjugated with FA.** Tri-functionalized GO-DETA was synthesized according to Yang and coworkers, through ring-opening reactions of epoxy groups on the surface of GO at room temperature.<sup>59</sup> In brief, GO (100 mg) and DETA (1.0 g) were dispersed in ethanol (100 mL, 95%) followed by 40 min sonication. After that the above mixture kept on stirring for 24 h at room temperature. The obtained suspension was filtered followed by washing for several times with ethanol, methanol and

acetone and finally dried in the vacuum overnight to obtained (GO-DETA).

In another step GO-DETA was modified with FA *via* amide reaction between COOH group of FA and NH<sub>2</sub> group of GO-DETA.<sup>60</sup> Briefly, FA (40 mg) was added into PBS (30 mL) and kept on continuous stirring for 2 h at room temperature. After that, EDC (0.9 mmol) and NHS (0.9 mmol) were added under magnetic stirring in the dark. Finally, GO-DETA suspension (1 mg mL<sup>-1</sup>) was added into the above solution followed by dialysis using dialysis membrane (molecular weight cutoff of 1000) and final product was left for dry at room temperature. Functionalization of GO surface is confirmed by XRD, FTIR, and Raman analysis.

**2.3.2 Synthesis of ZIF-8/GO-FA.** ZIF-8/GO-FA composite has been synthesized by the help of a previous reported work.<sup>61</sup> In brief, 95 mg of Zn(NO<sub>3</sub>)<sub>2</sub>·6H<sub>2</sub>O was dissolved in 50 mL of H<sub>2</sub>O under magnetic agitation for 15 min. Subsequently, 200 mg (2.43 mmol) of 2-methylimidazole in 50 mL of H<sub>2</sub>O was added to the above Zn(NO<sub>3</sub>)<sub>2</sub> solution at room temperature, followed by adding GO-FA suspension (1 mg mL<sup>-1</sup>) with magnetic agitation for another 1 h. Finally, the nanoparticles were collected by centrifugation and washing several times with ethanol and dried under vacuum at 60 °C for 6 h.

**2.3.3 Synthesis of DOX@ZIF-8/GO-FA/CP.** This DDDS has been synthesized by the help of reported method with some modification.<sup>5</sup> In brief, 95 mg of Zn(NO<sub>3</sub>)<sub>2</sub>·6H<sub>2</sub>O has been dissolved in 50 mL of H<sub>2</sub>O under magnetic agitation for 15 min, followed by adding 2 mL of DOX solution (2 mg mL<sup>-1</sup>). After 15 min, 200 mg (2.43 mmol) of 2-methylimidazole in 50 mL of H<sub>2</sub>O was added to the above solution at room temperature, with magnetic agitation for another 15 min to form a mixed suspension. Then, 1 mL of GO-FA suspension was added into the above solution and finally added 2 mL solution of CP (2 mg/



Scheme 1 Schematic protocol for the synthesis of DOX@ZIF-8/GO-FA/CP.

2 mL). After 1 h of reaction, the nanoparticles (DOX@ZIF-8/GO-FA/CP) were collected by centrifugation and washing several times with ethanol and then dried under vacuum at 60 °C for 6 h. The size, shape and charge of DOX@ZIF-8/GO-FA/CP have been analyzed by SEM, TEM, and zeta potential analysis. The synthesis process is outlined in Scheme 1. The same process has been applied for synthesis of ZIF-8/GO-FA for comparison.

#### 2.4 Loading and release profiles of DOX@ZIF-8/GO-FA/CP

The drug entrapment efficiency (EE%) and loading capacity (LC%) of ZIF-8/GO-FA, has been calculated by some modification of reported method.<sup>62</sup> Firstly, the drugs loaded ZIF-8/GO-FA has been digested in concentrated HCl and diluted with water followed by neutralization of solution with NaOH solution. This solution was further diluted with water to record the response of UV-vis spectroscopy for calculating the amount of DOX and CP at 488 nm and 265 nm, respectively against the standard drug solution with known concentration of DOX and CP. By using following equations EE% and LC% have been calculated.

$$EE (\%) = \frac{\text{weight of drug in nanocarrier}}{\text{weight of drug feed initially}} \times 100 \quad (1)$$

$$DL (\%) = \frac{\text{weight of drug in nanocarriers}}{\text{weight of nanocarrier}} \times 100 \quad (2)$$

To investigate the drug release behavior of drugs from the DOX@ZIF-8/GO-FA/CP nanocarrier, 2 mg of DOX@ZIF-8/GO-FA/CP nanoparticles has been dispersed in 10 mL of PBS solution (pH 7.4 or pH 5.0, separately to imitate the pH environment of normal body fluid and tumor tissue) followed by shaking at 100 rpm (37 °C) under dark conditions. 2 mL of the solution was collected at a regular time interval (0.5, 1, 2, 4, 8, 12, 24, 48, 72 h) for UV-vis analysis at the wavelength of 488 nm and 265 nm. To

maintain release of the drugs into the constant volume to attain constant evaluation concurrently, fresh PBS solution in same amount was added. All of the drug-releasing experiments were performed at 37 °C. The release of DOX and CP from ZIF-8/GO-FA was measured by UV-vis spectrum, and the release efficiency (RE) is calculated based on following eqn (3).

$$RE (\%) = \frac{\text{weight of released drug}}{\text{weight of loaded drug}} \times 100 \quad (3)$$

#### 2.5 Stability test

The stability test of drug loaded nanocarrier DOX@ZIF-8/GO-FA/CP has been investigated by calculating the RE (%) at regular time interval and measuring the particle size of DOX@ZIF-8/GO-FA/CP after storing at room temperature.

#### 2.6 Cell viability assays

Cell viability was determined using the MTT-assay, in which a yellow tetrazolium salt, [3-(4,5-dimethylthazol-2-yl)-2,5-diphenyltetrazolium bromide], was reduced into an insoluble formazan crystal (dark purple colour) in the reducing environment of living cells and measured at 570 nm using a microplate reader (Thermo Scientific). The reducing environment is lost in membrane compromised cells (apoptotic/necrotic cells), and the tetrazolium salt fails to reduce or formazan crystal formation. MCF-7 and MDA-MB-231 cells were seeded at density of  $5 \times 10^4$  cells per mL in 96-well plate, incubate for 24 h into CO<sub>2</sub> incubator. Cells treated with ZIF-8/GO-FA, DOX, CP, DOX + CP and DOX@ZIF-8/GO-FA/CP with 0 to 150 μM concentrations for 24 h. Here, MCF-10A cells were also used as control to check the toxicity of ZIF-8/GO-FA. After incubation 100 μL, 0.5 mg mL<sup>-1</sup> MTT solution in PBS was added into each well, and incubated for another 4 h. Cells were lysed with 100 μL of DMSO (dimethyl

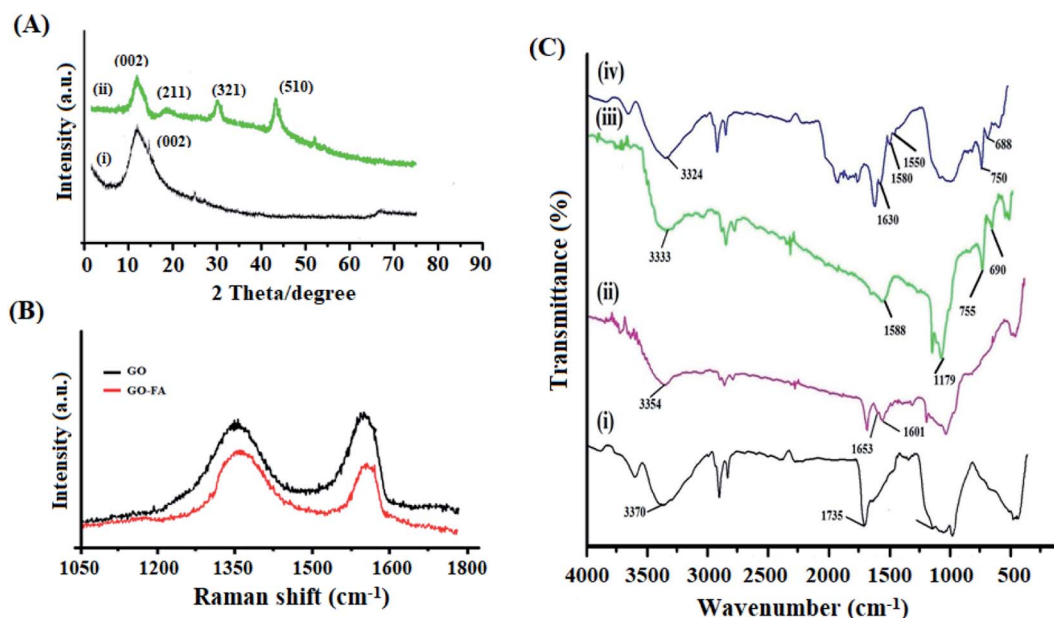


Fig. 1 (A) XRD spectra of (i) GO and (ii) GO-FA. (B) Raman analysis of GO and GO-FA. (C) FT-IR spectra of (i) GO, (ii) GO-FA, (iii) ZIF-8, and (iv) DOX@ZIF-8/GO-FA/CP.



sulfoxide). The optical density was measured at a wavelength of 570 nm in microplate reader. This experiment repeated thrice and the following equation was used to calculate the % cell viability:

$$\text{Cell viability (\%)} = \frac{\text{OD}_{\text{sample}}}{\text{OD}_{\text{control}}} \quad (4)$$

To determine inhibitory drug concentrations ( $\text{IC}_{50}$ ) to stop 50% cell growth, dose response curves of DOX, CP, the DOX + CP mixture and DOX@ZIF-8/GO-FA/CP were performed. The combination index (CI) for the DDSs was calculated by using the Chou-Talalay method.<sup>63,64</sup>

$$\text{CI} = \frac{\text{IC}_{50} \text{ of DOX in combination}}{\text{IC}_{50} \text{ of DOX}} + \frac{\text{IC}_{50} \text{ of CP in combination}}{\text{IC}_{50} \text{ of CP}} \quad (5)$$

In this analysis, synergy is defined ( $\text{CI} < 1$ ) and the smaller the CI is, the stronger the synergy is.

### 2.7 ROS generation and PI-staining

Reactive oxygen species (ROS) generation may cause oxidative damage inside the cells that initiate program cell death. ROS can be easily detected by using DCFDA. Which may increase due to toxicity of the xenobiotic compound. Propidium iodide (PI) cannot pass through the intact membrane of healthy cells. However, PI can enter into the cells through compromised cell membrane and stain the unhealthy cells. MCF-7 and MDA-MB-231 cell lines were cultured in DMEM media supplemented with 10% FBS and 1% Pen/Strep, and maintained in  $\text{CO}_2$  incubator at 37 °C temperature, 5%  $\text{CO}_2$  supply and humid air. MCF-7 and MDA-MB-231 cells ( $5 \times 10^4$  cells per mL) seeded into each well of 24 well plate, incubate for 24 h treated with ZIF-8/GO-FA, DOX, DOX@ZIF-8/GO-FA, and DOX@ZIF-8/GO-FA/CP of 50  $\mu\text{M}$  concentrations for 24 h then treated cells were allowed for staining with DCFDA (2.5  $\mu\text{M}$ ) and PI (10  $\mu\text{g mL}^{-1}$ ) in the separate experiment for 20 minutes. ROS generation and cell death were visualized in the inverted-fluorescence microscope at 20 $\times$  magnification (Radical Scientific).

## 3. Result and discussion

### 3.1 Spectroscopic characterizations for functionalized GO and DOX@ZIF-8/GO-FA/CP

The modification of GO sheets with DETA and FA has been analyzed by XRD analysis. In XRD spectrum of GO (Fig. 1A,

curve i), only one sharp peak at approximately  $11^\circ$  ( $d = 0.80$  nm), corresponding to the amorphous form of GO has been obtained, whereas after reacting with DETA and FA another peaks at  $18.36^\circ$  ( $d = 0.48$  nm),  $31^\circ$  and  $45^\circ$  are also appeared (Fig. 1A, curve ii). Besides, the (002) peak in the XRD spectrum of GO-FA, was narrower than that of pristine GO with decreased peak intensity, revealing a more aligned stacking of GO nano sheet and emergence of FA molecules.<sup>65,66</sup> It is reported that the emergence of peak at  $18.6^\circ$  due to certain degree of reduction by DETA and peaks at  $31^\circ$  and  $45^\circ$  belonging to the FA crystal structure during modification.<sup>59,67</sup> So that in XRD image, it is clearly visualized that GO sheets exfoliated by DETA and decorated by FA. As a proof of concept, modification of GO sheets with FA molecules, Raman analysis has been done because it is a powerful technique to characterize the structural of carbon-based material like as carbon nanotube or graphene. In the Raman spectrum of graphene (Fig. 1B), two characteristic peaks at  $\sim 1352$   $\text{cm}^{-1}$  and  $\sim 1592$   $\text{cm}^{-1}$  have been obtained as D and G band. The D band corresponds to the degree of disorder or defects in the carbon lattice of the GO, while the G-band is assigned due to the bond stretching of  $\text{sp}^2$  hybridized carbon pairs in the GO basal plane.<sup>68,69</sup> Whereas after modification with FA, these two bands have also been obtained at  $\sim 1355$   $\text{cm}^{-1}$  and  $\sim 1596$   $\text{cm}^{-1}$ . The intensity ratio ( $I_{\text{D}}/I_{\text{G}}$ ) of GO-FA was found to be higher (1.14) than GO (0.91), implying the increase of  $\text{sp}^3$ -bonded carbon atoms and the decrease of conjugated structure.<sup>70–72</sup>

Furthermore FT-IR spectra also confirmed the modification of GO sheets (Fig. 1C). In the spectrum of GO, the peak around 3370  $\text{cm}^{-1}$  and 1733  $\text{cm}^{-1}$  were assigned to O–H and C=O stretching vibration of hydroxyl and carboxyl groups, respectively (Fig. 1C, curve i).<sup>73</sup> Besides this, after modification of GO sheets with DETA and FA additional peaks at 1653  $\text{cm}^{-1}$  and 1601  $\text{cm}^{-1}$ , are belonging to amide bands (I & II) in GO-FA spectrum (Fig. 1C, curve ii), which performed the successfully conjugation of FA on GO sheets.<sup>67</sup> Whereas, FT-IR analysis also confirmed the interaction between ZIF-8 and GO-FA in ZIF-8/GO-FA and DOX@ZIF-8/GO-FA/CP nanoparticles. In the spectrum of ZIF-8 (Fig. 1C, curve iii), the peaks at 2925  $\text{cm}^{-1}$ , 1588  $\text{cm}^{-1}$  and 1179  $\text{cm}^{-1}$  are attributed to C–H, C=N and C–N stretching vibrations, respectively. Moreover, the peaks at 754  $\text{cm}^{-1}$  and 690  $\text{cm}^{-1}$  were assigned to Zn–O and Zn–N of ZIF-8, respectively, which confirm the complexation between Zn metal and imidazole linker.<sup>38</sup> However, in case of DOX@ZIF-8/GO-FA/CP, IR-spectrum (Fig. 1C, curve iv), the intensity of the peak at 1733  $\text{cm}^{-1}$  decreased, indicating that the carboxyl

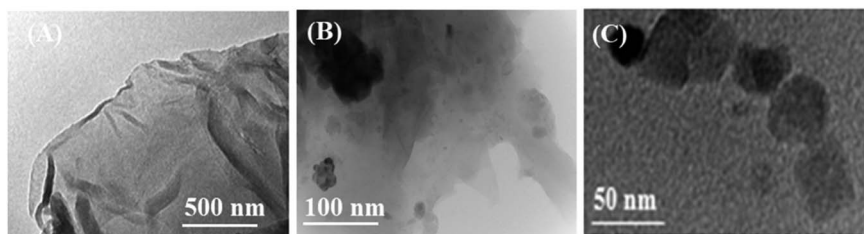


Fig. 2 TEM images of GO (A), GO-FA (B), and DOX@ZIF-8/GO-FA/CP (C).



groups of GO interacted with  $\text{Zn}^{2+}$  and further confirming the successful growth of ZIF-8 on the GO sheet.<sup>67</sup> Along with this, the peaks of O–H stretching in GO spectra, amide I, amide II in GO–FA, C=N, Zn–O, and Zn–N in ZIF-8 spectra shifted downward after DOX and CP loading in DOX@ZIF-8/GO–FA spectrum, like as 3310, 1630, 1580, 1550, 750, and 688  $\text{cm}^{-1}$  respectively, confirmed the loading of DOX and CP molecules with ZIF-8/GO–FA nanocarrier.

### 3.2 Surface morphology and size distribution

The morphology of GO, GO/FA and DOX@ZIF-8/GO–FA/CP have been analyzed by TEM and SEM analysis (Fig. 2 & 3). In Fig. 2A transparent sheets with wrinkles has been obtained for exfoliated and oxidized GO. Besides this, in Fig. 2B some visible dark patches indicate the modification of GO sheets with DETA and FA as earlier reported.<sup>74</sup> Meanwhile, the TEM image of modified GO also demonstrates that the modification of GO by DETA followed by FA causes no significant damage to the microstructure of GO sheet. Furthermore, spherical like structures have been obtained for drugs loaded nanoparticles (DOX@ZIF-8/GO–FA/CP) Fig. 2C & 3B. *In situ* growth of ZIF-8 on the surface of GO sheet reveals morphology consistent with previous reports.<sup>75</sup> SEM images also validate the TEM result (Fig. 3A and B). The particle size of nanocarrier has been evaluated by SEM and TEM analysis (DOX@ZIF-8/GO–FA/CP) as 45–60 nm (Fig. 2C & 3B). Whereas, the particle size distribution measured by using DLS were a little bigger ( $68 \pm 4$  nm) than those observed using SEM and TEM, which might be attributed to a solvation layer around the nanoparticles for DLS measurements (Fig. 3C). The elemental distributions on DOX@ZIF-8/GO–FA/CP illustrated in

Fig. 3D. Besides this, zeta potential was also evaluated for confirmation of GO–FA functionalization on ZIF-8 surface. The lower value of zeta potential for ZIF-8/GO–FA (–6.55 mV) than ZIF-8 (34.1 mV) revealed out the modification of ZIF-8 with GO–FA due to the presence of more carboxylic acid group in GO–FA molecule.<sup>76</sup>

### 3.3 Encapsulation efficiency and drug loading profile

UV-vis absorption spectra could verify the modification of GO with FA molecules, as well as DOX and CP loading in the ZIF-8/GO–FA nanoparticles. In Fig. 4A we obtained a peak at 267 nm for FA, however after conjugation with GO sheets, a downward shift has been obtained at 255 nm, which confirmed the formation of GO–FA as reported earlier.<sup>70</sup> Whereas, free DOX and CP have characteristic absorbance peaks at 488 and 265 nm respectively, which could be clearly observed on the spectrum of DOX@ZIF-8/GO–FA/CP nanoparticles (Fig. 4A), and GO–FA and ZIF-8 show no peak in this region. This indicates that DOX and CP are encapsulated in the ZIF-8/GO–FA nanoparticles during the synthesis procedure. After applying digestion process the concentration of DOX and CP has been measured and percentage of EE and LC has been calculated by using eqn (1) & (2). Loading and encapsulation efficiencies were estimated as 17.5% and 87% for DOX and 10.6% and 53.0% for CP, respectively.

### 3.4 *In vitro* drug release from DOX@ZIF-8/GO–FA/CP nanoparticles

To investigate the drug releasing profile of DOX and CP from DOX@ZIF-8/GO–FA/CP nanoparticles, drug release experiments

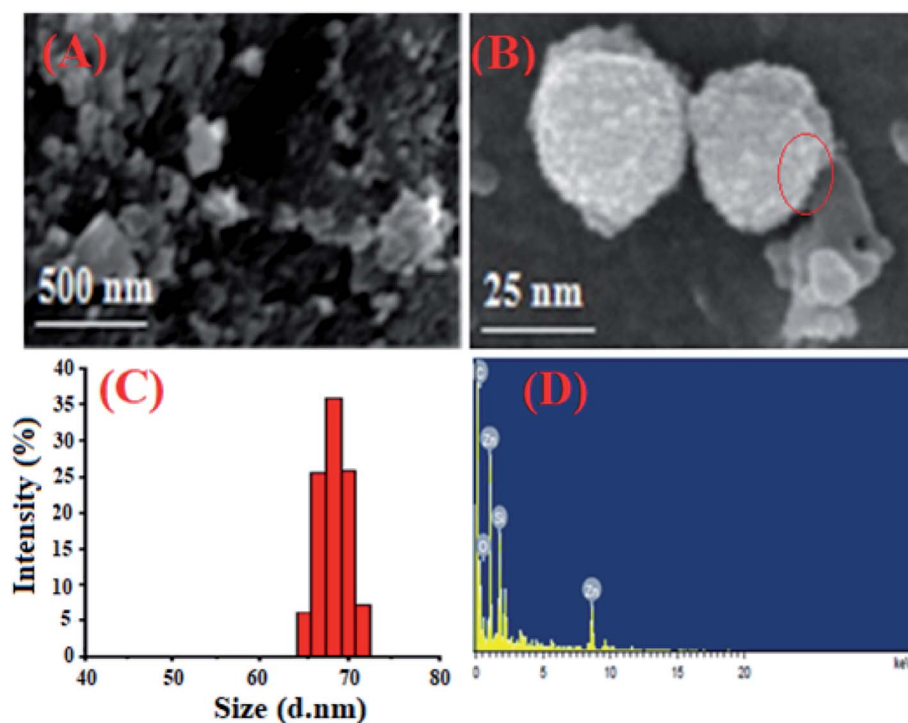
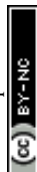


Fig. 3 SEM images of GO–FA (A), and DOX@ZIF-8/GO–FA/CP (B). DLS image of DOX@ZIF-8/GO–FA/CP (C). EDS image of DOX@ZIF-8/GO–FA/CP (D).



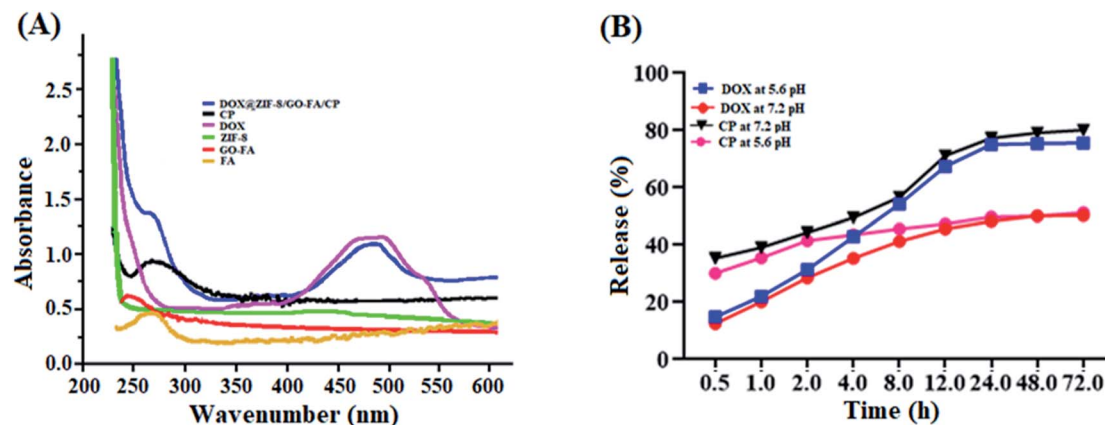


Fig. 4 (A) UV-vis spectra of FA, GO-FA, ZIF-8, DOX, CP, and DOX@ZIF-8/GO-FA/CP suspensions. (B) *In vitro* drug release profiles of DOX and CP from ZIF-8@DOX/GO-FA/CP in phosphate buffer saline (PBS) at pH 7.2 and 5.6 separately.

has been performed in PBS at acidic (pH = 5.6) and neutral (pH = 7.2). It is interestingly that the release of DOX and CP from DOX@ZIF-8/GO-FA/CP exhibited similar pH-responsive behavior at both pH, as shown in Fig. 4B. At pH 5.6, about 76% of DOX and 80% of CP has been released after 72 h, whereas 50% of both drugs released at pH 7.2, suggesting that DOX and CP can be released at a much faster rate in a more acidic environment than a neutral environment. It is reported that in neutral conditions (pH 7.4) ZIF-8 nanoparticles are stable and can easily decompose under acidic conditions.<sup>5</sup> These results showed the non-covalent interactions of DOX and CP with ZIF-8/GO-FA nanoparticles and higher drug releasing behavior of CP than DOX has been exhibited because of surface interaction of CP molecules with GO-FA, whereas DOX molecules have been encapsulated in the pores of ZIF-8 in DOX@ZIF-8/GO-FA/CP nanoparticles.

### 3.5 Stability test of DOX@ZIF-8/GO-FA/CP nanocarrier

The stability of the proposed DOX@ZIF-8/GO-FA/CP nanocarrier was also examined by performing releasing experiment after 5 h, on every fifth day, over the period of four weeks

(Fig. 5A) and calculating RE% using eqn (3). The burst effect of drugs has been obtained after one month, at room temperature. The burst effect of drugs showed the degradation of ZIF-8 crystal after gaining some moisture. Zhang *et al.*, reported that the degradation of ZIF-8 structures after being immersed in water for different time periods and as a result ZIF-8 crystals almost destroyed the entire crystallite.<sup>77</sup> So that within fourth week ZIF-8 crystallite destroyed and ultimate burst effect of drugs have been obtained in *in vitro* study, means the total drug released in 5 h from DOX@ZIF-8/GO-FA/CP nanocarrier. DLS study has also been done to compare the size of the DOX@ZIF-8/GO-FA/CP nanocarrier after one month, and size variation (65–90 nm) has been obtained which show the stability of DOX@ZIF-8/GO-FA/CP nanocarrier up to one month (Fig. 5B).

### 3.6 Enhanced effects of combination therapy delivered by ZIF-8/GO-FA nanocarrier

MTT-assay was used to assess cell viability in MCF-7 and MDA-MB-231 cells using the protocols described in the material and methods. Toxicity of the ZIF-8/GO-FA nanocarrier was found to be negligible in MCF-7, and MDA-MB-231 cells. It means

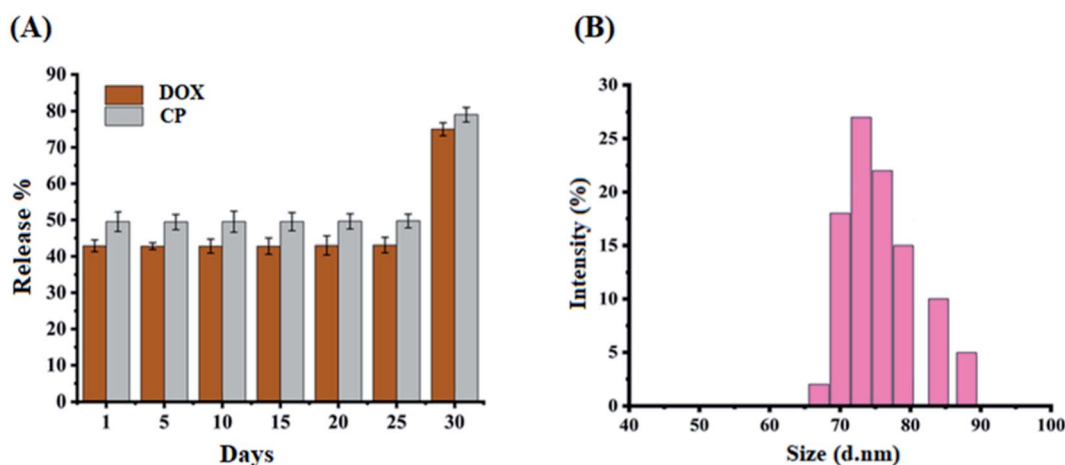


Fig. 5 Stability analysis of DOX@ZIF-8/GO-FA/CP, (A) releasing behavior for stability of DOX@ZIF-8/GO-FA/CP after 5 h, on every fifth day, over the period of four weeks, and (B) DLS image for particle size of DOX@ZIF-8/GO-FA/CP after one month.

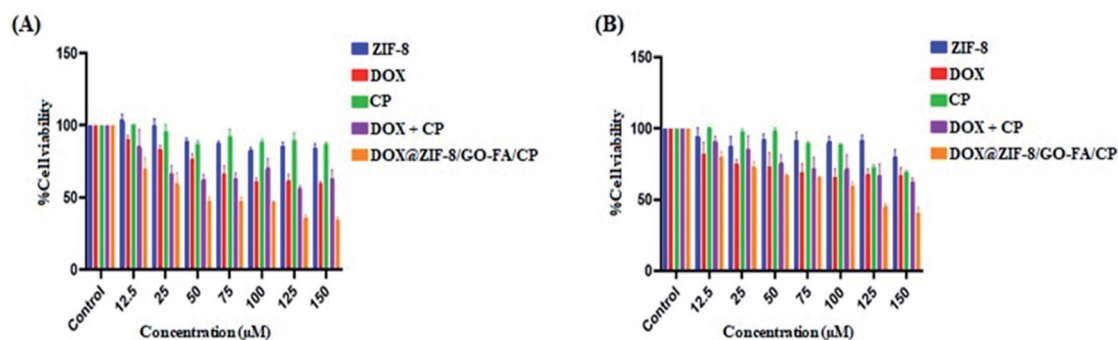


Fig. 6 Cell viability of (A) MCF-7 and (B) MDA-MB-231 cells incubated with ZIF-8, DOX, CP, DOX + CP, and DOX@ZIF-8/GO-FA/CP.

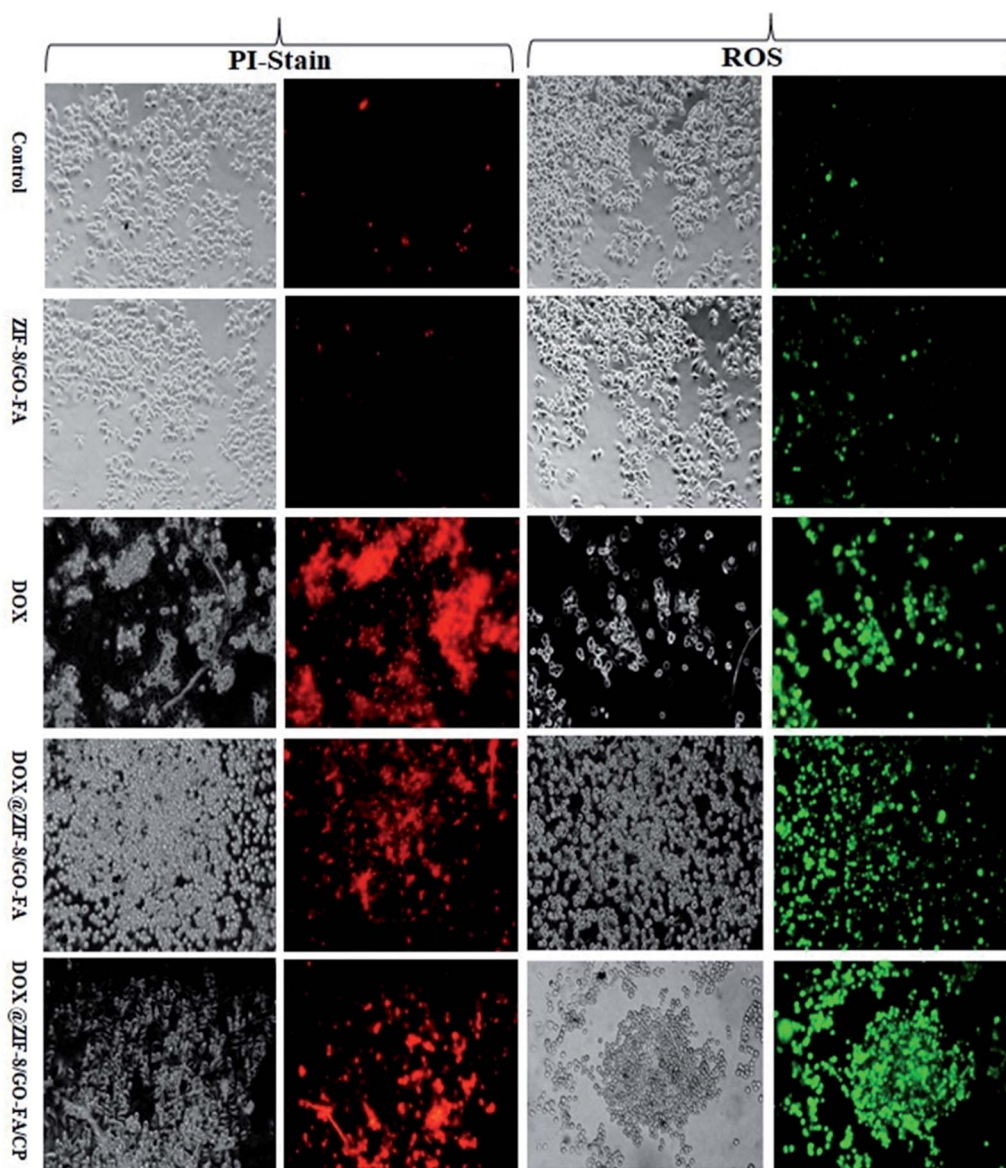


Fig. 7 Fluorescence microscope images of PI-staining and ROS-generation in MCF-7 cells after 24 h incubation with control, ZIF-8/GO-FA, DOX, DOX@ZIF-8/GO-FA, and DOX@ZIF-8/GO-FA/CP at 20 $\times$  magnification.



nanocarrier is not toxic. Fig. 6 shows the inhibitory effect of individual drug molecules and in conjugation with nanocarrier on MCF-7 and MDA-MB-231 cells lines. Half maximal inhibitory concentration ( $IC_{50}$ ) values have been calculated by reported method and obtained as: 163.22 and 218  $\mu$ M for DOX; 1245 and 535  $\mu$ M for CP; 175.61 and 193.34  $\mu$ M for DOX + CP; 41.99 and 116  $\mu$ M for DOX@ZIF-GO-FA/CP on MCF-7 and MDA-MB-231 cells, respectively. The lower  $IC_{50}$  value of DOX@ZIF-GO-FA/CP nanoparticles indicated better cytotoxicity on cancerous cell lines. Besides this CI values of DOX@ZIF-GO-FA/CP is <1 (0.29 and 0.75 for MCF-7 and MDA-MB-231 cells, respectively) showed synergistic effect. Hence these results suggested that our synthesized DOX@ZIF-GO-FA/CP nanocarrier had excellent, controlled cytostatic effects and promising anti-tumor efficacy.

### 3.7 Enhanced cell death in DOX@ZIF-8/GO-FA/CP treated cells

PI staining and ROS generation were evaluated, to show the synergistic effect of both drugs, in combination with ZIF-8/

GO-FA. Because of the cytotoxic effect of drugs and drug combinations, propidium iodide enters into the cells *via* a damaged cell membrane. ROS are generated as a result of drug action, initiating programmed cell death. We observed that a few cells in MCF-7 and MDA-MB-231 cells produced ROS and stain with PI due to the ZIF-8/GO-FA nanocarrier. Whereas, DOX treated cells showed most of the cells have been generated ROS and stained with PI in MCF-7 as well as MDA-MB-231 cells. However, nanocarrier encapsulated DOX (DOX@ZIF-8/GO-FA) treated cells showed controlled ROS generation and PI uptake. Furthermore, when DOX is combined with CP in ZIF-8/GO-FA, and given the treatment in both cell lines, increased ROS generation and PI uptake were observed. This study favours combination of DOX and CP when encapsulated and conjugated with ZIF-8/GO-FA for their synergistic cytotoxic effects as compared to the single DOX encapsulated nanocarrier (Fig. 7 and 8, and also see ESI† Fig. 1–4).

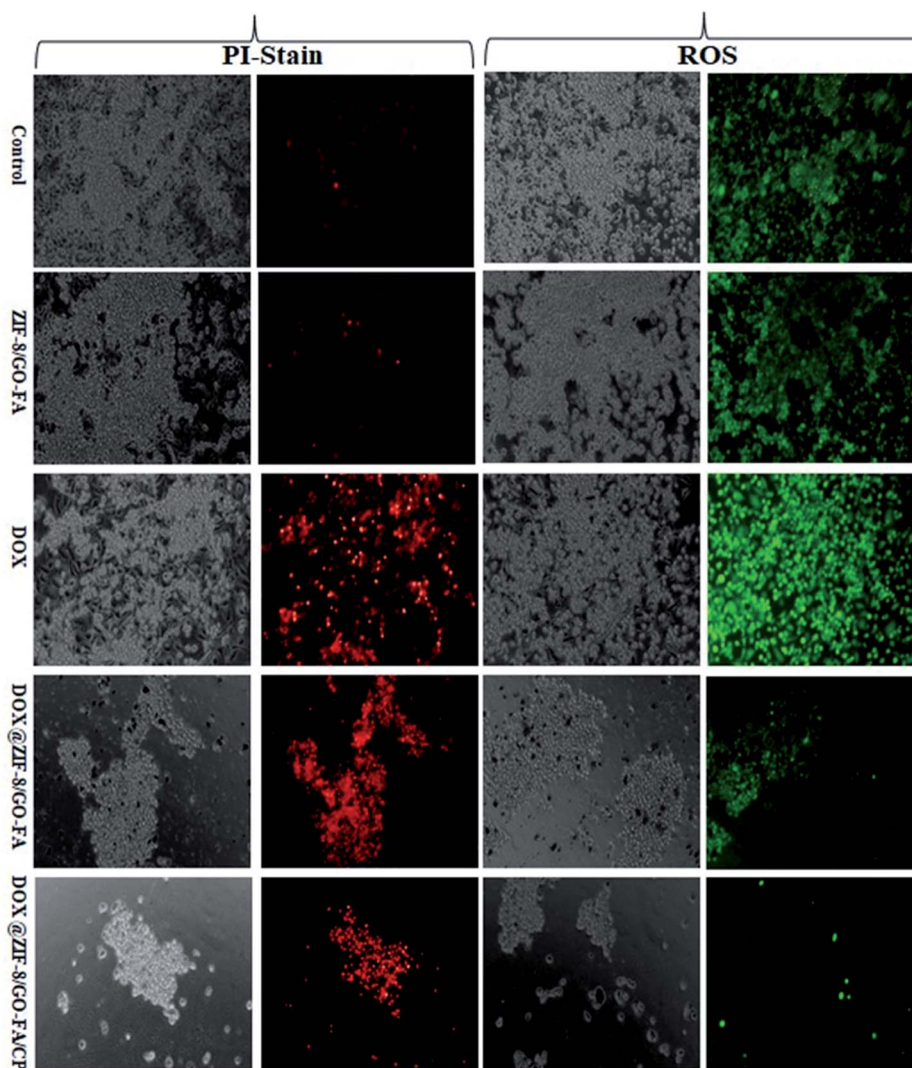


Fig. 8 Fluorescence microscope images of PI-staining and ROS-generation in MDA-MB-231 cells after 24 h incubation with control, ZIF-8/GO-FA, DOX, DOX@ZIF-8/GO-FA, and DOX@ZIF-8/GO-FA/CP at 20 $\times$  magnification.

## 4. Conclusions

An ingenious method was developed as GO-FA functionalized MOF based nanosystem and successfully used for delivery of DOX and CP in combination (DOX@ZIF-8/GO-FA/CP). This MOF/GO-FA system showed negligible cytotoxicity and excellent biocompatibility. More interestingly, the FA-modification enhanced the drug uptake in breast cancer cells and the DOX@ZIF-8/GO-FA/CP nanosystem showed clear selection towards cancer cells and avoid healthy cells. This nanosystem showed their synergistic cytotoxic effect on MCF-7 and MDA-MB-231 cells, due to controlled release of DOX and CP on specific site under acidic condition. We also expect that the design of the pH-responsive nanosystem can give new inspiration to the synthesis of nanoparticles with multifunctional application. The practical application of this study at *in vitro* level, the synthesized nanoformulations might be used as dual drug delivery system in breast cancer treatment for chemotherapeutic drugs such as doxorubicin and cyclophosphamide *etc.* Result of this study may be validated on animal model as well as on clinical setup.

## Funding

The project was supported by the Indian Council of Medical Research, India in 2019, No. 3/1/3/PDF(19)/2019-HRD.

## Conflicts of interest

Authors declare that they have no conflict of interest.

## Acknowledgements

I want to thank that Indian Council of Medical Research for providing Post-Doctoral fellowship, National Institute of Cancer Prevention and Research for providing lab facility to conduct proposed work. I want to thank DCRS INMAS, DRDO and CSIR-NPL for providing data analysis facility.

## References

- 1 J. Liao, Y. Song, C. Liu, D. Li, H. Zheng and B. Lu, *Polym. Chem.*, 2019, **10**, 5879–5893.
- 2 W. Xiao, X. Zeng, H. Lin, K. Han, H.-Z. Jia and X.-Z. Zhang, *Chem. Commun.*, 2015, **51**, 1475–1478.
- 3 J.-L. Li, L. Jiang, B.-W. Wang, J.-L. Tian, W. Gu, X. Liu and S.-P. Yan, *New J. Chem.*, 2015, **39**, 529–538.
- 4 K. Cho, X. Wang, S. Nie, Z. Chen and D.-M. Shin, *Clin. Cancer Res.*, 2008, **14**, 1310–1316.
- 5 Z. Tian, X. Yao, K. Ma, X. Niu, J. Grothe, Q. Xu, L. Liu, S. Kaskel and Y. Zhu, *ACS Omega*, 2017, **2**, 1249–1258.
- 6 W.-Z. Li, X.-L. Hao, N. Zhao, W.-X. Han, X.-F. Zhai, Q. Zhao, Y.-E. Wang, Y.-Q. Zhou, Y.-C. Cheng, Y.-H. Yue, L.-N. Fu, J.-L. Zhou, H.-Y. Wu and C.-J. Dong, *J. Controlled Release*, 2016, **226**, 107–114.
- 7 X. Hu, Y. Zhang, H. Zhou and H. Wan, *J. Appl. Polym. Sci.*, 2015, **132**, 42623.
- 8 D. M. Eckmann, R. J. Composto, A. Tsourkas and V. R. Muzykantov, *J. Mater. Chem. B*, 2014, **2**, 8085–8097.
- 9 R. Khandelia, S. Bhandari, U. N. Pan, S. S. Ghosh and A. Chattopadhyay, *Small*, 2015, **11**, 4075–4081.
- 10 M. I. Majeed, Q. Lu, W. Yan, Z. Li, I. Hussain, M. N. Tahir, W. Tremel and B. Tan, *J. Mater. Chem. B*, 2013, **1**, 2874–2884.
- 11 M. Karimi, H. Mirshekari, M. Aliakbari, P. Sahandi-Zangabad and M. R. Hamblin, *Nanotechnol. Rev.*, 2016, **5**, 195–207.
- 12 S. Chen, X. Hao, X. Liang, Q. Zhang, C. Zhang, G. Zhou, S. Shen, G. Jia and J. Zhang, *J. Biomed. Nanotechnol.*, 2016, **12**, 1–27.
- 13 T. Zhou, J. Li and P. Liu, *Colloids Surf., A*, 2018, **553**, 180–186.
- 14 X. Li, V. M. Garamus, N. Li, Y. Gong, Z. Zhe, Z. Tian and A. Zou, *Colloids Surf., A*, 2018, **548**, 61–69.
- 15 W. Hao, D. Liu, Y. Wang, X. Han, S. Xu and H. Liu, *Colloids Surf., A*, 2018, **537**, 446–451.
- 16 L. Kong, F. Zhang, P. Xing, X. Chu and A. Hao, *Colloids Surf., A*, 2017, **522**, 577–584.
- 17 L. Liu, J. Zeng, X. Zhao, K. Tian and P. Liu, *Colloids Surf., A*, 2017, **526**, 48–55.
- 18 L. Tong, Y. Yang, X. Luan, J. Shen and X. Xin, *Colloids Surf., A*, 2017, **522**, 470–476.
- 19 M. X. Wu and Y. W. Yang, *Adv. Mater.*, 2017, **29**, 1606134.
- 20 J. Park, Q. Jiang, D. Feng, L. Mao and H. C. Zhou, *J. Am. Chem. Soc.*, 2016, **138**, 3518–3525.
- 21 J. M. Yang, Q. Liu and W.-Y. Sun, *Microporous Mesoporous Mater.*, 2014, **190**, 26–31.
- 22 I. A. Lazaro, S. Haddad, S. Sacca, C. O. Tavra, D. F. Jimenez and R. S. Forgan, *Chem*, 2017, **2**, 561–578.
- 23 R. C. Huxford, J. D. Rocca and W. B. Lin, *Curr. Opin. Chem. Biol.*, 2010, **14**, 262–268.
- 24 M. R. Broadley, P. J. White, J. P. Hammond, I. Zelko and A. Lux, *New Phytol.*, 2007, **173**, 677–702.
- 25 S. R. Venna, J. B. Jasinski and M. A. Carreon, *J. Am. Chem. Soc.*, 2010, **132**, 18030–18033.
- 26 J. S. Kahn, L. Freage, N. Enkin, M. A. A. Garcia and I. Willner, *Adv. Mater.*, 2017, **29**, 1602782–1602787.
- 27 Y. Duan, F. Ye, Y. Huang, Y. Qin, C. Hea and S. Zhao, *Chem. Commun.*, 2018, **54**, 5377–5380.
- 28 J. Zhuang, C.-H. Kuo, L.-Y. Chou, D.-Y. Liu, E. Weerapana and C.-K. Tsung, *ACS Nano*, 2014, **8**, 2812–2819.
- 29 C. Zheng, Y. Wang, S. Z. F. Phua, W. Q. Lim and Y. Zhao, *ACS Biomater. Sci. Eng.*, 2017, **3**, 2223–2229.
- 30 M. Zheng, S. Liu, X. Guan and Z. Xie, *ACS Appl. Mater. Interfaces*, 2015, **7**, 22181–22187.
- 31 A. R. Chowdhuri, D. Laha, S. Pal, P. Karmakar and S. K. Sahu, *Dalton Trans.*, 2016, **45**, 18120–18132.
- 32 H. Ren, L. Zhang, J. An, T. Wang, L. Li, X. Si, L. He, X. Wu, C. Wang and Z. Su, *Chem. Commun.*, 2014, **50**, 1000–1002.
- 33 P. Horcajada, T. Chalati, C. Serre, B. Gillet, C. Sebrie, T. Baati, J. F. Eubank, D. Heurtaux, P. Clayette, C. Kreuz, J.-S. Chang, Y. K. Hwang, V. Marsaud, P.-N. Bories, L. Cynober, S. Gil, G. Férey, P. Couvreur and R. Gref, *Nat. Mater.*, 2009, **9**, 172–178.
- 34 W. Cai, C.-C. Chu, G. Liu and Y.-X. Wang, *Small*, 2015, **11**, 4806–4822.



- 35 N. Liédana, A. Galve, C. Rubio, C. Téllez and J. Coronas, *ACS Appl. Mater. Interfaces*, 2012, **4**, 5016–5021.
- 36 C. Adhikari, A. Das and A. Chakraborty, *Mol. Pharmaceutics*, 2015, **12**, 3158–3166.
- 37 L. Gao, Q. Chen, T. Gong, J. Liu and C. Li, *Nanoscale*, 2019, **11**, 21030–21045.
- 38 C. Adhikari, A. Das and A. Chakraborty, *Mol. Pharmaceutics*, 2015, **12**, 3158–3166.
- 39 H. Zheng, Y. Zhang, L. Liu, W. Wan, P. Guo, A. M. Nystrom and X. Zou, *J. Am. Chem. Soc.*, 2016, **138**, 962–968.
- 40 Q. Wu, M. Niu, X. Chen, L. Tan, C. Fu, X. Ren, J. Ren, L. Li, K. Xu, H. Zhong and X. Men, *Biomaterials*, 2018, **162**, 132–143.
- 41 R. Bian, T. Wang, L. Zhang, L. Li and C. Wang, *Biomater. Sci.*, 2015, **3**, 1270–1278.
- 42 L. Yan, X. Chen, Z. Wang, X. Zhang, X. Zhu, M. Zhou, W. Chen, L. Huang, V. A. L. Roy, P. K. N. Yu, G. Zhu and W. J. Zhang, *ACS Appl. Mater. Interfaces*, 2017, **9**, 32990–33000.
- 43 X. Chen, M. Zhang, S. Li, L. Li, L. Zhang, T. Wang, M. Yu, Z. C. Mou and C. Wang, *J. Mater. Chem. B*, 2017, **5**, 1772–1778.
- 44 J. Feng, Z. Xu, P. Dong, W. Q. Yu, F. Liu, Q. Y. Jiang, F. A. Wang and X. Q. Liu, *J. Mater. Chem. B*, 2019, **7**, 994–1004.
- 45 H. Y. Zhang, Q. Li, R. L. Liu, X. K. Zhang, Z. G. Li and Y. X. Luan, *Adv. Funct. Mater.*, 2018, **28**, 1802830.
- 46 N. Liédana, A. Galve, C. Rubio, C. Téllez and J. Coronas, *ACS Appl. Mater. Interfaces*, 2012, **4**, 5016–5021.
- 47 H. Zheng, Y. Zhang, L. Liu, W. Wan, P. Guo, A. M. Nyström and X. Zou, *J. Am. Chem. Soc.*, 2016, **138**, 962–968.
- 48 F. T. Boyle and G. F. Costello, *Chem. Soc. Rev.*, 1998, **27**, 251–261.
- 49 M. A. Seyed, I. Jantan, S. N. A. Bukhari and K. Vijayaraghavan, *J. Agric. Food Chem.*, 2016, **64**, 725–737.
- 50 S.-L. Chen, *Appl. Sci.*, 2017, **7**, 25.
- 51 T. H. Tran, H. T. Nguyen, T. T. Pham, J. Y. Choi, H.-G. Choi, C. S. Yong and J. O. Kim, *ACS Appl. Mater. Interfaces*, 2015, **7**, 28647–28655.
- 52 U. Hess, S. Shahabi, L. Treccani, P. Streckbein, C. Heiss and K. Rezwani, *Mater. Sci. Eng., C*, 2017, **77**, 427–435.
- 53 X. Guo, Z. Zhao, D. Chen, M. Qiao, F. Wan, D. Cun, Y. Sun and M. Yang, *Asian J. Pharm. Sci.*, 2019, **14**, 78–85.
- 54 S. Wu, X. Yang, Y. Lu, Z. Fan, Y. Li, Y. Jiang and Z. Hou, *Drug Delivery*, 2017, **24**, 51–60.
- 55 S. Dhanavel, T. A. Revathy, T. Sivarajani, K. Sivakumar, P. Palani, V. Narayanan and A. Stephen, *Polym. Bull.*, 2020, **77**, 213–233.
- 56 J. Liao, Y. Song, C. Liu, D. Li, H. Zheng and B. Lu, *Polym. Chem.*, 2019, **10**, 5879.
- 57 J. H. Lee and A. Nan, *J. Drug Delivery*, 2012, 915375.
- 58 K. Sun, L. Li, X. L. Yu, L. Liu, Q. Meng, F. Wang and R. Zhang, *J. Colloid Interface Sci.*, 2017, **486**, 128–135.
- 59 A. Yang, J. Li, C. Zhang, W. Zhang and N. Ma, *Appl. Surf. Sci.*, 2015, **346**, 443–450.
- 60 S. Feng, J. Pan, C. Li and Y. Zheng, *Nanotechnology*, 2020, **31**(13), 135701.
- 61 J. Zhuang, C.-H. Kuo, L.-Y. Chou, D.-Y. Liu, E. Weerapana and C.-K. Tsung, *ACS Nano*, 2014, **8**, 2812–2819.
- 62 X.-G. Wang, Z.-Y. Dong, H. Cheng, S.-S. Wan, W.-H. Chen, M.-Z. Zou, J.-W. Huo, H.-X. Deng and X.-Z. Zhang, *Nanoscale*, 2015, **7**(38), 16061–16070.
- 63 J. Zhu, X. Xu, M. Hu and L. Qiu, *J. Biomed. Nanotechnol.*, 2015, **11**, 997–1006.
- 64 L. Ma, M. Kohli and A. Smith, *ACS Nano*, 2013, **7**, 9518–9525.
- 65 N. Maslekar, R. A. M. Noor, R. P. Kuchel, Y. Yao, P. B. Zetterlund and V. Agarwal, *Nanoscale Adv.*, 2020, 1–16.
- 66 J. Guo, H. Bao, Y. Zhang, X. Shen, J.-K. Kim, J. Ma and L. Shao, *J. Membr. Sci.*, 2021, **619**, 118791.
- 67 Y. Ye, X. Mao, J. Xu, J. Kong and X. Hu, *Int. J. Polym. Sci.*, 2019, 8453493.
- 68 G. Eda and M. Chhowalla, *Adv. Mater.*, 2010, **22**, 2392–2415.
- 69 A. C. Ferrari and J. Robertson, *Philos. Trans. R. Soc. London*, 2004, **362**, 2477–2512.
- 70 L. Zhan, Y. Zhang, Q. L. Zeng, Z. D. Liu and C. Z. Huang, *J. Colloid Interface Sci.*, 2014, **426**, 293–299.
- 71 Y. Cai, Y. Fadil, F. Jasinski, S. C. Thickett, V. Agarwal and P. B. Zetterlund, *Carbon*, 2019, **149**, 445–451.
- 72 Z. Sun, L. Zhao, C. Liud, Y. Zhen, W. Zhang and J. Ma, *Chem. Eng. J.*, 2019, **372**, 896–904.
- 73 L. J. Yang, B. B. Tang and P. Y. Wu, *J. Mater. Chem. A*, 2015, **3**, 15838–15842.
- 74 M. d'Sousa, L. A. V. d'Luna, L. C. Fonseca, S. Giorgio and O. L. Alves, *ACS Appl. Nano Mater.*, 2018, **1**, 922–932.
- 75 M. Jahan, Z. L. Liu and K. P. Loh, *Adv. Funct. Mater.*, 2013, **23**, 5363–5372.
- 76 P. Jiang, Y. Hu and G. Li, *Talanta*, 2019, **200**, 212–217.
- 77 H. Zhang, D. Liu, Y. Yao, B. Zhang and Y. S. Lin, *J. Membr. Sci.*, 2015, **485**, 103–111.

